

Variance-Adaptive Muon: Accelerating LLM Pretraining with NSR-Modulated and Variance-Scaled Momentum

Jingru Li¹, Yibo Fan¹, Huan Li¹

¹College of Artificial Intelligence, Nankai University

{jingru_lee, yibofan}@mail.nankai.edu.cn, lihuanss@nankai.edu.cn

Abstract

Large Language Models (LLMs) achieve competitive performance across diverse natural language processing (NLP) tasks, yet pretraining is computationally demanding, making optimizer efficiency an important practical consideration. Muon accelerates LLM pretraining via orthogonal momentum updates that serve as a matrix analogue of the element-wise sign operator. Motivated by the recent perspective that Adam is a variance-adaptive sign update algorithm, we propose two variants of Muon, **Muon-NSR** and **Muon-VS**, which apply variance-adaptive normalization to momentum before orthogonalization. Muon-NSR applies noise-to-signal ratio (NSR) modulation, while Muon-VS performs variance-based scaling without introducing additional hyperparameters. Experiments on GPT-2 and LLaMA pretraining demonstrate that our proposed methods accelerate convergence and consistently achieve lower validation loss than both competitive, well-tuned AdamW and Muon baselines. For example, on the LLaMA-1.2B model, Muon-NSR and Muon-VS reduce the iterations required to reach the target validation loss by 1.36 \times relative to the well-tuned Muon following the recent benchmark [Wen *et al.*, 2025].

1 Introduction

Deep learning, particularly Transformer-based Large Language Models (LLMs), has become a dominant paradigm in modern natural language processing (NLP), enabling substantial gains across a wide range of tasks [Yang *et al.*, 2025; Comanici *et al.*, 2025; Guo *et al.*, 2025]. Central to this success is the regime of extensive self-supervised pretraining on massive corpora, which serves as the fundamental catalyst for the emergence of sophisticated reasoning and few-shot generalization capabilities [Raffel *et al.*, 2020; Brown *et al.*, 2020; Kaplan *et al.*, 2020]. However, given that such scaling incurs immense computational costs often spanning thousands of GPU-hours, enhancing the convergence speed and sample efficiency of the underlying optimizer has emerged as a paramount research priority [Schneider *et al.*, 2019; Kaplan *et al.*, 2020; Hoffmann *et al.*, 2022].

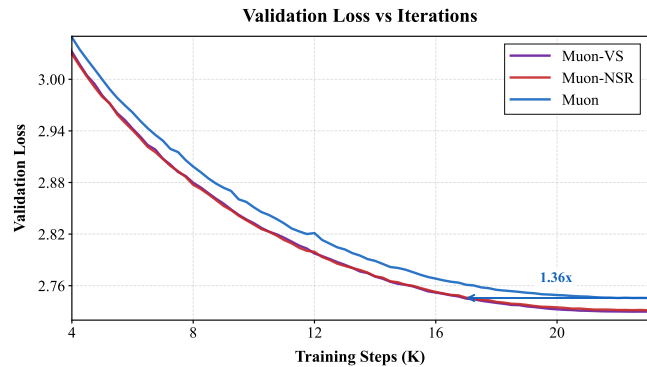


Figure 1: Validation loss trajectories for **LLaMA-1.2B** on C4-en (Suite B). The plot illustrates the convergence of **Muon-NSR**, **Muon-VS**, and well-tuned **Muon** following the recent benchmark [Wen *et al.*, 2025] over training iterations, with the model pre-trained on the DCLM dataset under 1 \times Chinchilla compute budget.

Adam and its variants constitute the de facto standard for LLM pretraining and have dominated deep learning training for the past decade [Zhang *et al.*, 2020; Kunstner *et al.*, 2023]. Recent theoretical insights suggest that, under equal EMA decay rates, Adam operates effectively as a variance-adaptive sign update, dynamically attenuating steps in high-variance regimes [Orvieto and Gower, 2025]. On the other hand, challenging Adam’s dominance, the recently introduced Muon optimizer [Jordan *et al.*, 2024] employs Newton–Schulz (NS) iterations to approximate the orthogonal polar factor. By flattening the singular value spectrum to unity, Muon serves as a matrix-valued analogue of the sign update, preserving directional structure while strictly normalizing magnitude. Motivated by the correspondence between Adam’s scalar variance adaptation and Muon’s matrix-level updates, the following question emerges:

Can variance-adaptive components be integrated into Muon to achieve acceleration similar to the improvements that Adam provides for scalar sign updates?

Contributions. To address the above question, this work proposes **Muon-NSR** and **Muon-VS**, two variance-adaptive extensions of the Muon. Our main contributions are:

- **Variance-adaptive variants.** We introduce Muon-NSR and Muon-VS, which integrate adaptive variance statis-

tics into the orthogonal update structure. Muon-NSR employs explicit noise-to-signal ratio (NSR) modulation, while Muon-VS implements parameter-free variance scaling. Both approaches apply variance statistics before the Newton–Schulz (NS) step to preserve the matrix-signed update form.

- **Superior empirical efficiency.** Experimental results on GPT-2 and LLaMA pretraining demonstrate that the proposed variants achieve faster convergence and lower validation loss compared to well-tuned baselines, while requiring only a single additional buffer. For example, Muon-NSR and Muon-VS reduce the number of iterations required to reach the target validation loss on LLaMA-1.2B by $1.36\times$ relative to the well-tuned Muon following the recent benchmark [Wen *et al.*, 2025].

2 Related Works

Stochastic Gradient Descent (SGD) [Robbins and Monroe, 1951] and its momentum-augmented variant, Stochastic Gradient Descent with Momentum (SGDM) [Polyak, 1964], serve as the cornerstones of deep learning optimization. While these methods rely on dense gradient information, a parallel line of research explores sign-based optimization to enhance communication and computational efficiency. By decoupling the update direction from its magnitude, these methods align with steepest descent in L_∞ geometry [Leplat *et al.*, 2025]. For instance, SignSGD [Bernstein *et al.*, 2018] employs element-wise signs to compress gradients to 1-bit, significantly reducing communication overhead while maintaining convergence rates comparable to SGD. Extending this paradigm, Signum [Bernstein *et al.*, 2018] and Lion [Chen *et al.*, 2023] integrate momentum into this framework by applying the sign operator to accumulated gradient statistics, thereby combining the efficiency of 1-bit compression with the stability of momentum.

However, relying on a global learning rate, SGD and sign-based methods struggle to adapt to the significant block-wise sharpness disparity inherent in Transformer architectures [Wang *et al.*, 2025]. To address this, adaptive gradient methods rescale updates using historical gradient statistics. AdaGrad [Duchi *et al.*, 2011] pioneered this approach by normalizing updates via accumulated squared gradients, though it suffers from a premature decay of the effective learning rate. This limitation is mitigated by RMSProp [Tieleman and Hinton, 2012] and Adam [Kingma, 2014], which utilize exponential moving averages (EMA) of second moments. AdamW [Loshchilov and Hutter, 2017] further refines this by decoupling weight decay from the gradient-based update. Due to its robustness, AdamW has been widely adopted in modern Large Language Model (LLM) training pipelines [Zhang *et al.*, 2020; Kunstner *et al.*, 2023] and serves as a primary baseline for this work.

Despite their success, standard adaptive methods operate in a coordinate-wise manner, effectively approximating the Hessian as a diagonal matrix and ignoring correlations between parameters [Martens and Grosse, 2020; Yao *et al.*, 2021]. To capture clearer structural information, geometry-aware optimizers exploit the matrix structure of parameters. Sham-

poo [Gupta *et al.*, 2018] introduces Kronecker-factored preconditioners to efficiently approximate full-matrix second-moment scaling. Advancing this paradigm, SOAP [Vyas *et al.*, 2024] employs eigen-decomposition to refine the approximation of the local loss geometry. For matrix-valued parameters specifically, Muon [Jordan *et al.*, 2024] orthogonalizes update directions via efficient Newton–Schulz (NS) iterations, achieving orthogonal updates with constrained singular values. Recent studies demonstrate that Muon scales effectively to LLM training [Liu *et al.*, 2025], with further efficiency gains achievable through adaptive magnitude control mechanisms, as proposed in AdaMuon [Si *et al.*, 2025] and NorMuon [Li *et al.*, 2025].

3 Motivation from the Variance-Adaptive Perspective of Adam

An equivalent form of Adam with equal betas. The classical Adam consists of the following steps

$$m_t = \beta_1 m_{t-1} + (1 - \beta_1)g_t, \quad (1)$$

$$v_t = \beta_2 v_{t-1} + (1 - \beta_2)g_t^2, \quad (2)$$

$$d_t = \frac{m_t}{\sqrt{v_t}} = \frac{m_t}{\sqrt{m_t^2 + v_t - m_t^2}}, \quad (3)$$

$$x_{t+1} = x_t - \eta d_t. \quad (4)$$

Since Adam applies adaptive preconditioning coordinate-wise, the above steps focus on a single scalar component with stochastic gradient $g_t \in \mathbf{R}$. We also omit bias correction and the stability term ε for analytical tractability. Recently, Orvieto and Gower [2025] empirically observed that employing a shared EMA decay rate for both first- and second-moment estimators, denoted as $\beta_1 = \beta_2 = \beta$, maintains competitive performance across various settings. Under this shared parameterization, Orvieto and Gower [2025, Proposition 1] proved that $v_t - m_t^2$ satisfies the following recursion

$$v_t - m_t^2 = \beta(v_{t-1} - m_{t-1}^2) + \beta(1 - \beta)(m_{t-1} - g_t)^2. \quad (5)$$

Replacing (2) by (5) yielding an equivalent form.

Interpretation of Adam as variance-adaptive sign update. Let the stochastic gradient sample g_t at iteration t be modeled as a realization drawn from a Gaussian distribution with unknown, slowly varying parameters: $g_t \sim \mathcal{N}(\mu, \sigma^2)$. Let $(\mu_{t-1}, \sigma_{t-1}^2)$ denote the estimate of the gradient’s mean and variance from the previous iteration. Upon observing g_t , we define the updated estimate (μ_t, σ_t^2) as the solution to the following regularized maximum likelihood estimation problem [Orvieto and Gower, 2025]

$$\begin{aligned} (\mu_t, \sigma_t^2) = \arg \min_{\mu \in \mathbf{R}, \sigma^2 > 0} & \left\{ -\log p(g_t | \mu, \sigma^2) \right. \\ & \left. + \frac{1}{\lambda} \text{KL}(\mathcal{N}(\mu_{t-1}, \sigma_{t-1}^2) \| \mathcal{N}(\mu, \sigma^2)) \right\}, \end{aligned} \quad (6)$$

where $\lambda > 0$ is a regularization coefficient governing the trade-off between maximizing the likelihood of the current observation and minimizing the divergence from the previous estimate. The Gaussian negative log-likelihood is given by

$$-\log p(g_t | \mu, \sigma^2) = \frac{1}{2} \log \sigma^2 + \frac{(g_t - \mu)^2}{2\sigma^2},$$

and the Kullback–Leibler divergence from the prior estimate $(\mu_{t-1}, \sigma_{t-1}^2)$ to the candidate distribution is

$$\begin{aligned} \text{KL}(\mathcal{N}(\mu_{t-1}, \sigma_{t-1}^2) \parallel \mathcal{N}(\mu, \sigma^2)) \\ = \frac{1}{2} \left[\frac{\sigma_{t-1}^2}{\sigma^2} + \frac{(\mu_{t-1} - \mu)^2}{\sigma^2} - 1 - \log \left(\frac{\sigma_{t-1}^2}{\sigma^2} \right) \right]. \end{aligned}$$

Letting $\beta = \frac{1}{1+\lambda} \in (0, 1)$, Orvieto and Gower [2025, Theorem 4.1] proved that the minimizer of (6) admits a closed-form solution recursively defined as follows

$$\mu_t = \beta \mu_{t-1} + (1 - \beta) g_t, \quad (7)$$

$$\sigma_t^2 = \beta \sigma_{t-1}^2 + \beta(1 - \beta)(m_{t-1} - g_t)^2. \quad (8)$$

Comparing (5) with (8) and (1) with (7) reveals that $\sigma_t^2 = v_t - m_t^2$ and $\mu_t = m_t$, implying that m_t and $v_t - m_t^2$ in Adam’s updates serve as online estimators of the local gradient mean and variance, respectively. Substituting into Adam’s update rule (3) yields a variance-adaptive formulation defined by

$$d_t = \frac{m_t}{\sqrt{m_t^2 + \sigma_t^2}} = \frac{\text{sign}(m_t)}{\sqrt{1 + \sigma_t^2/m_t^2}}, \quad (m_t \neq 0), \quad (9)$$

where the term $\sigma_t/|m_t|$ represents the local noise-to-signal ratio (NSR). This derivation characterizes Adam as a Signum update [Bernstein *et al.*, 2018] modulated by an NSR-dependent damping factor, thereby suppressing step sizes in noise-dominated regimes [Orvieto and Gower, 2025].

Muon: A Matrix Analogue of Signum. The design of Muon [Jordan *et al.*, 2024] generalizes Signum by transitioning from element-wise scalar normalization to spectral normalization, thereby preserving the intrinsic correlations within the parameter matrix. Formally, let $W_t \in \mathbf{R}^{m \times n}$ and $G_t \in \mathbf{R}^{m \times n}$ denote the parameter matrix and the stochastic gradient at iteration t . The Muon optimizer maintains a momentum estimate M_t and computes updates using a matrix-valued sign operator $\text{msign}(\cdot)$ with decoupled weight decay according to the recursion

$$\begin{aligned} M_t &= \beta M_{t-1} + G_t, \\ O_t &= \text{msign}(\beta M_t + G_t) \in \mathbf{R}^{m \times n}, \\ W_t &= W_{t-1} - \eta_t (O_t + \lambda W_{t-1}), \end{aligned} \quad (10)$$

where $\beta \in [0, 1]$ is the EMA decay rate and η_t denotes the learning rate. The $\text{msign}(\cdot)$ operator distinguishes this method by computing the orthogonal polar factor of the matrix. Specifically, for a singular value decomposition (SVD) $M = U \Sigma V^\top$ containing the singular value matrix Σ , the operator is defined by

$$\text{msign}(M) = U V^\top.$$

Mathematically, this corresponds to replacing Σ with the identity matrix, which flattens the spectrum of the momentum matrix. This spectral normalization serves as a matrix-valued analogue to the scalar sign operation employed in Signum [Jordan *et al.*, 2024; Chen *et al.*, 2025].

Algorithm 1 Muon-NSR and Muon-VS

Require: Parameters $W_0 \in \mathbf{R}^{m \times n}$; learning rate η ; weight decay λ ; EMA rate β (shared for first and second moments, i.e., $\beta_1 = \beta_2 = \beta$); variance-sensitivity γ ; stabilizer ε ; Newton–Schulz iterations K ; optimizer type (Muon-NSR or Muon-VS).

1: $M_0 \leftarrow 0$, $\Gamma_0 \leftarrow 0$
2: **for** $t = 1, 2, \dots$ **do**
3: $G_t = \text{Stochastic Gradient Oracle}(W_{t-1})$
4: $\Gamma_t \leftarrow \beta \Gamma_{t-1} + \beta(1 - \beta)(M_{t-1} - G_t)^{\odot 2}$
5: $M_t \leftarrow \beta M_{t-1} + (1 - \beta)G_t$
6: $\widehat{M}_t \leftarrow \frac{M_t}{1 - \beta^t}$, $\widehat{\Gamma}_t \leftarrow \frac{\Gamma_t}{1 - \beta^t}$
7: $\tilde{M}_t \leftarrow G_t + \frac{\beta}{1 - \beta} \widehat{M}_t$
8: **if** type is Muon-NSR **then**
9: $\overline{M}_{NSR,t} \leftarrow \frac{\tilde{M}_t}{\sqrt{\tilde{M}_t^{\odot 2} + \gamma \widehat{\Gamma}_t + \varepsilon}}$ {Muon-NSR}
10: **else**
11: $\overline{M}_{VS,t} \leftarrow \frac{\tilde{M}_t}{\sqrt{\widehat{\Gamma}_t + \varepsilon}}$ {Muon-VS}
12: **end if**
13: $O_t \leftarrow \text{NS}_K(\overline{M}_{NSR,t} \text{ or } \overline{M}_{VS,t})$
14: $W_t \leftarrow W_{t-1}(1 - \eta \lambda) - \eta s_{\text{scale}} O_t$
15: **end for**

Motivation: Muon with variance-adaptive scaling. The reformulation in (9) identifies the core mechanism of Adam as a sign update algorithm modulated by variance-adaptive scaling. In contrast, Muon generalizes this sign operation to the matrix domain via spectral normalization. Hence, this theoretical disconnect motivates integrating Adam’s variance adaptation into the Muon framework.

4 Muon-NSR and Muon-VS

Building upon the aforementioned motivation, this paper presents two variance-adaptive extensions of the Muon optimizer, namely **Muon-NSR** and **Muon-VS**. Both variants incorporate variance adaptivity into the matrix update while preserving the spectral normalization structure of Muon. The complete procedure is given in Algorithm 1.

Momentum and Variance. At iteration t , we maintain two coupled exponential moving statistics that follow the derivation in Section 3. The momentum estimator M_t is updated by (7), which yields a smoothed estimate of the local gradient mean under a shared EMA decay rate and provides the directional signal for the subsequent polar-factor computation. In parallel, the variance surrogate Γ_t is updated by (8). This recursion depends on the elementwise squared $(G_t - M_{t-1})^{\odot 2}$, which measures the deviation of the current stochastic gradient from the previous mean estimate. As a result, Γ_t captures dispersion around the evolving mean rather than accumulating second moments in Adam. The pair (M_t, Γ_t) then supplies the mean and variance information required by the normalization step used before applying the matrix sign operator.

Nesterov-style acceleration. To incorporate Nesterov momentum consistent with the Muon optimizer, we derive an extrapolated update direction. While Muon updates its momentum by directly adding the current gradient as shown in

the first line of (10), our formulation instead maintains momentum as an EMA, as defined on line 5 of Algorithm 1. Consequently, relative to Muon, the contribution of each past gradient to M_t is uniformly scaled by $(1 - \beta)$. To recover the Muon-consistent weighting in the Nesterov extrapolation, we therefore normalize the momentum term by $(1 - \beta)^{-1}$, yielding the lookahead direction

$$\tilde{M}_t = G_t + \frac{\beta}{1 - \beta} M_t.$$

This normalization removes the attenuation introduced by the EMA parameterization, so that the resulting Nesterov-style direction is directly comparable to the Muon formulation.

Muon-NSR The Muon-NSR variant normalizes Muon’s update by integrating both \tilde{M}_t and $\hat{\Gamma}_t$, which is motivated by (9). The update rule is formally expressed as

$$\overline{M}_{NSR,t} = \frac{\tilde{M}_t}{\sqrt{\tilde{M}_t^{\odot 2} + \gamma \hat{\Gamma}_t + \varepsilon}}, \quad (11)$$

where $\gamma \geq 0$ modulates the sensitivity to variance and $\varepsilon > 0$ ensures numerical stability. By neglecting the stability term ε , this expression permits an analytical reformulation. For coordinates characterized by non-zero mean magnitudes, the normalized update is approximated by the following expression

$$\overline{M}_{NSR,t} \approx \frac{\text{sign}(\tilde{M}_t)}{\sqrt{1 + \gamma \frac{\hat{\Gamma}_t}{\tilde{M}_t^{\odot 2}}}},$$

which characterizes the optimizer as a soft-gating mechanism with a noise-to-signal (NSR) ratio. This formulation effectively suppresses coordinate-wise updates where the estimated uncertainty is high relative to the signal strength, thereby facilitating more conservative steps along high-noise directions. Furthermore, applying this normalization prior to the Newton–Schulz orthogonalization ensures that the intended spectral structure of the update remains uncorrupted. In Section 5.3, we present an ablation study that incorporates NSR adaptivity after orthogonalization.

Muon-VS. The Muon-VS variant implements variance-scaled normalization

$$\overline{M}_{VS,t} = \frac{\tilde{M}_t}{\sqrt{\hat{\Gamma}_t + \varepsilon}}. \quad (12)$$

Relative to Muon-NSR, this formulation simplifies the denominator by removing the squared-mean term $\tilde{M}_t^{\odot 2}$ and the associated sensitivity parameter γ . This offers a practical advantage that streamlines the hyperparameter search space by eliminating γ , while retaining the principled mechanism of variance-based damping. Since constant scaling does not affect orthogonalization, Muon-VS can be regarded as a variant of Muon-NSR with huge γ such that $\gamma \hat{\Gamma}_t \gg \tilde{M}_t^{\odot 2}$.

Orthogonalization and Parameter Update Given the preconditioned update matrix \overline{M}_t (either $\overline{M}_{NSR,t}$ in (11) or $\overline{M}_{VS,t}$ in (12)), we obtain an orthogonal update direction by

applying Muon’s Newton–Schulz (NS) orthogonalization operator:

$$O_t \leftarrow \mathbf{NS}_K(\overline{M}_t).$$

Here, $\mathbf{NS}_K(\cdot)$ denotes K iterations of Newton–Schulz (NS), which yields an efficient approximation to the orthogonal polar factor of \overline{M}_t [Jordan *et al.*, 2024; Liu *et al.*, 2025].

Finally, we apply decoupled weight decay with learning rate η and weight decay coefficient λ , together with a dimension-dependent scaling factor. Depending on the experimental setting, we use one of the following two definitions for s_{scale}

$$s_{scale} = 0.2 \sqrt{\max(m, n)} \quad \text{or} \quad s_{scale} = \sqrt{\max\left(1, \frac{m}{n}\right)},$$

where 0.2 is the scale constant in [Liu *et al.*, 2025], and m and n denote the dimensions of W_t , respectively. To ensure a fair and rigorous evaluation, we maintain consistency by employing the identical scaling factor that corresponds to each specific experimental configuration in the Muon baselines.

Computational and Spatial Complexity In terms of computational complexity, Muon-NSR and Muon-VS introduce auxiliary variance-adaptive update procedures requiring $O(mn)$ operations. The execution time for these procedures is significantly shorter than the $O(m^2n)$ latency incurred by the Newton–Schulz iteration. Regarding space complexity, the proposed variants require storing variance estimates as element-wise buffers. While this necessitates an additional auxiliary buffer for each parameter, the overall memory footprint remains consistent with standard Adam-type optimizers.

5 Experiments

We conduct experiments to verify the efficiency of the proposed methods. The source code is publicly available at <https://github.com/jingru-lee/Variance-Adaptive-Muon>.

5.1 GPT-2 Pretraining

Setup. We evaluate the performance of five optimizers for GPT-2 pretraining [Radford *et al.*, 2019] utilizing the AdaMuon codebase [Si *et al.*, 2025], which is built upon NanoGPT [Karpathy, 2022]. Concretely, we train GPT-2 Small (124M) and GPT-2 Medium (350M) models on the OpenWebText dataset [Gokaslan *et al.*, 2019], employing the standard GPT-2 tokenizer. Adhering to the training configuration detailed in [Si *et al.*, 2025, Section 4.1], we adopt a learning rate schedule consisting of a 2,000-step linear warmup followed by a constant learning rate phase. All models are trained for 100,000 steps with a context length of 1,024 and an effective batch size of 480 sequences, corresponding to a total compute budget of approximately 49.2 billion tokens.

We benchmark AdamW, Muon, and AdaMuon against our proposed variants, Muon-NSR and Muon-VS. Regarding hyperparameters, we use $(\beta_1, \beta_2) = (0.9, 0.95)$ for AdamW, while for all Muon-based methods, we set the momentum $\beta = 0.95$. Additionally, for Muon-NSR, we set $\gamma = 10$. To ensure a fair comparison, all methods utilize a peak learning rate of 6×10^{-4} , a weight decay of 0.1, and a gradient clipping threshold of 1.0. Further experimental details are provided in Appendix A.1.

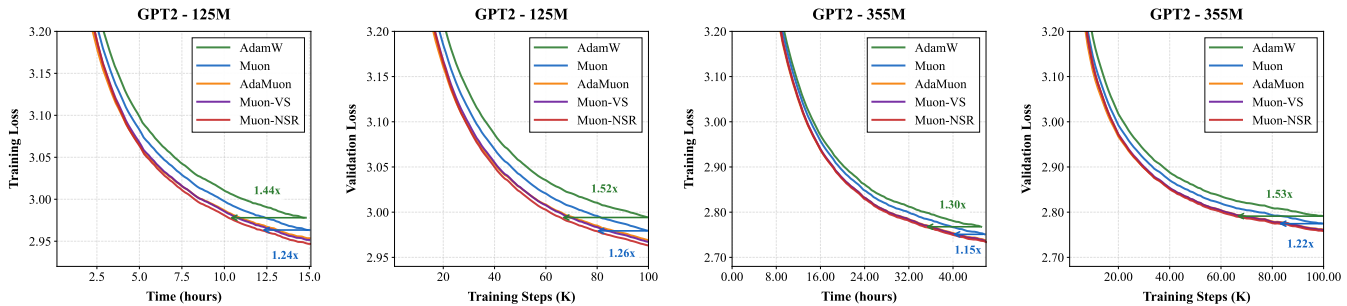


Figure 2: Comparison of training and validation loss curves on **GPT-2 125M** and **GPT-2 355M** under the setting of [Si *et al.*, 2025]. Curves are smoothed via exponential moving average (EMA, decay=0.95) for improved visual clarity.

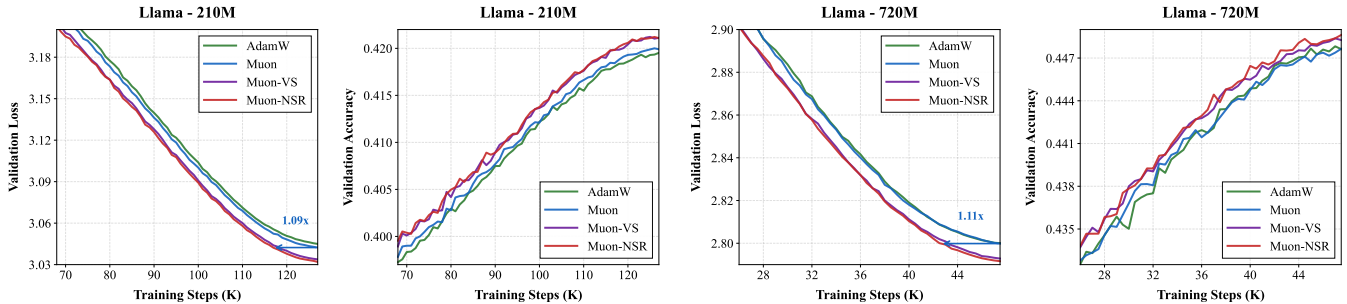


Figure 3: Comparison of validation loss and next-token top-1 accuracy on **LLaMA-130M** and **LLaMA-300M** under the Suite B protocol following the benchmark [Wen *et al.*, 2025].

Results. The experimental results are summarized in Figure 2, which plots training loss against wall-clock time and validation loss against training steps for both GPT-2 Small (124M) and Medium (350M). Most notably, Muon-NSR achieves superior performance across all metrics. In terms of computational efficiency, measured by the reduction in training loss relative to wall-clock time, Muon-NSR exhibits the fastest convergence rate. This indicates that the computational overhead introduced by the spectral refinement is negligible compared to the substantial optimization gains. Furthermore, regarding sample efficiency as evidenced by the validation loss trajectory over training steps, Muon-NSR attains the lowest terminal loss, suggesting enhanced generalization capabilities. Additionally, Muon-VS consistently outperforms both the AdaMuon and Muon baselines throughout the training process.

5.2 LLaMA Pretraining

To assess the generalization of our algorithm across standard LLaMA-based pretraining regimes, we conduct two complementary experimental suites, each closely following an established training recipe: Suite A follows [Semenov *et al.*, 2025], and Suite B follows [Wen *et al.*, 2025]. Since both benchmarks incorporate extensive hyperparameter tuning, they serve as rigorous and competitive baselines.

Suite A: We adopt the standardized LLaMA pretraining framework from [Semenov *et al.*, 2025], utilizing its official codebase for model architecture, data preprocessing, and training protocols. The models are decoder-only Transfor-

mers featuring SwiGLU activations, RMSNorm, RoPE positional encodings, tied input/output embeddings, and bias-free linear layers. We evaluate two specific configurations: a 210M-parameter model ($d_{\text{model}} = 768$, $L = 24$, $H = 12$) and a 720M-parameter model ($d_{\text{model}} = 2048$, $L = 12$, $H = 16$). Following the benchmark protocol, we pretrain on a cleaned and deduplicated 100B-token subset of FineWeb [Penedo *et al.*, 2024]. The data is tokenized using the GPT-2 tokenizer with a context length of 512 tokens employed for both training and evaluation.

Regarding optimization, the 210M model employs an effective batch size of 256 sequences and is trained for 128k steps (approx. 16.8B tokens). The 720M model scales the batch size to 1,984 sequences, training for 48k steps (approx. 48B tokens). To ensure a fair comparison, we strictly retain the benchmark’s tuned hyperparameters as detailed in [Semenov *et al.*, 2025, Appendix E], including the learning rate schedules, warmup strategy, weight decay, and gradient clipping thresholds. Full experimental details are provided in Appendix A.2. In this controlled environment, we benchmark AdamW and Muon, and against our proposed variants, Muon-NSR and Muon-VS.

Suite A Results. Figure 3 visualizes the training dynamics by plotting validation loss and next-token top-1 accuracy against training steps, where accuracy is defined as the fraction of token positions for which the model’s highest-probability prediction matches the ground truth. Across both Llama-210M and Llama-720M configurations, our proposed variants, Muon-NSR and Muon-VS, consistently maintain a

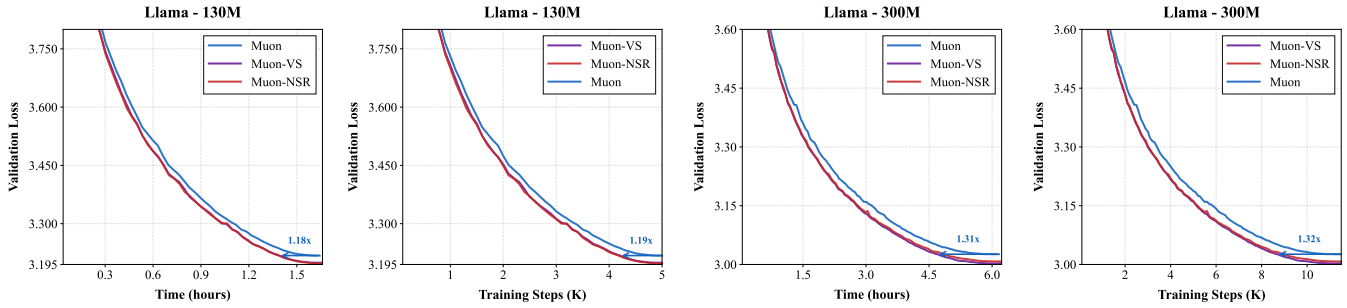


Figure 4: Comparison of validation loss curves on **LLaMA-130M** and **LLaMA-300M** under the Suite B protocol following the benchmark [Wen *et al.*, 2025].

Table 1: Final validation loss for Suite A benchmarks upon completion of the compute budget. Δ_{AdamW} denotes the absolute loss reduction relative to the AdamW baseline (higher is better). The **Improvement Ratio** normalizes the gain of each specific optimizer (‘opt’) against the gain achieved by the standard Muon baseline: $\Delta_{\text{AdamW}}(\text{opt})/\Delta_{\text{AdamW}}(\text{Muon})$.

Optimizer	Final loss \downarrow	$\Delta_{\text{AdamW}} \uparrow$	Impr. Ratio \uparrow
Llama-210M			
AdamW	3.0458	—	—
Muon	3.0418	0.0040	1.0 \times (Base)
Muon-NSR	3.0322	0.0136	3.40\times
Muon-VS	3.0330	0.0128	3.20 \times
Llama-720M			
AdamW	2.7879	—	—
Muon	2.7858	0.0021	1.0 \times (Base)
Muon-NSR	2.7806	0.0073	3.48 \times
Muon-VS	2.7798	0.0081	3.86\times

superior optimization trajectory compared to AdamW and the standard Muon baseline throughout the entire pretraining process. Table 1 quantifies the final performance at the conclusion of the fixed compute budget. While the standard Muon optimizer yields only marginal gains over AdamW, our variants collectively achieve significantly larger reductions in validation loss, delivering improvement ratios of **3.2 \times to 3.8 \times** relative to the Muon baseline across different model scales.

Suite B. We follow the rigorously tuned pretraining protocol of [Wen *et al.*, 2025, Appendix C], which emphasizes regime-specific hyperparameter optimization to ensure fair benchmarking. Our implementation is built upon the codebase from [Liang *et al.*, 2024], reproducing the training recipes and learning rate schedules reported in [Wen *et al.*, 2025]. Under this standardized 1 \times Chinchilla token-budget setup, we benchmark Muon against our variants, Muon-NSR and Muon-VS. To isolate the efficacy of our proposed modifications, our variants **inherit** the base Muon hyperparameters. Regarding model architecture, we train three LLaMA-family decoder-only Transformers with a fixed depth of 32 layers and a sequence length of 4,096: Llama-130M, Llama-300M, and Llama-1.2B. In contrast to the data mixture used in [Wen *et al.*, 2025], we pretrain exclusively on the DCLM dataset, and all downstream evaluations are conducted on C4-en using

the LLaMA-2 tokenizer. Full experimental details are provided in Appendix A.3.

Suite B Results. We present the comparative training dynamics for Llama-130M and Llama-300M in Figure 4, and for the scaled-up Llama-1.2B model in Figure 1. The results demonstrate that our proposed variants, Muon-NSR and Muon-VS, consistently outperform the Muon baseline across all three model scales, even under the rigorously hyperparameter-optimized protocol of [Wen *et al.*, 2025]. Crucially, the superior convergence rates observed in the step-wise plots translate directly into tangible practical benefits, as evidenced by the relative performance ranking being strictly preserved in the wall-clock time comparisons (Figure 4). Most notably, our approach exhibits excellent scalability to larger architectures. As highlighted in Figure 1, on the largest Llama-1.2B configuration, Muon-VS significantly improves sample efficiency, reducing the number of training iterations required to reach the target validation loss by a factor of **1.36 \times** relative to the Muon baseline.

Discussions. We only compare with Muon and AdamW as the baselines. As the benchmarks [Semenov *et al.*, 2025; Wen *et al.*, 2025] provide a comprehensive evaluation demonstrating the superiority of Muon over other alternatives, and given our alignment with their experimental protocol, repeating these comparisons is redundant. Furthermore, compared with AdamW, the additional computational cost incurred by the Newton-Schulz (NS) iterations in Muon-class optimizers is practically negligible. As empirically demonstrated in Figure 18 of benchmark [Semenov *et al.*, 2025], this overhead can be effectively amortized through engineering optimizations, such as parallel execution, ensuring that the algorithmic convergence gains translate directly into wall-clock speedups.

5.3 Ablation Studies

Sensitivity to the variance coefficient γ . We investigate the sensitivity of Muon-NSR to the coefficient γ ((11)), which governs the strength of the variance-adaptive modulation relative to the squared mean term $\tilde{M}_t^{\odot 2}$. To isolate the impact of γ , we conduct a parameter sweep while holding all other hyperparameters, model architectures, and training schedules constant. Table 2 summarizes the final evaluation loss and the relative improvement over the respective baselines (AdaMuon for GPT-2 and Muon for LLaMA-130M).

Table 2: Sensitivity analysis of the variance-sensitivity coefficient γ in Muon-NSR. The table reports the final evaluation loss and the improvement (Δ) relative to the respective architecture-specific baselines (AdaMuon for GPT-2; Muon for LLaMA-130M).

Optimizer	Final Eval Loss	Δ
GPT-2		
AdaMuon (Baseline)	2.9571	–
Muon-NSR ($\gamma = 1$)	2.9531	+0.0041
Muon-NSR ($\gamma = 10$)	2.9506	+0.0065
Muon-NSR ($\gamma = 100$)	2.9536	+0.0036
Muon-NSR ($\gamma = 1000$)	2.9545	+0.0026
LLaMA-130M		
Muon (Baseline)	3.2179	–
Muon-NSR ($\gamma = 0.1$)	3.2181	-0.0002
Muon-NSR ($\gamma = 1$)	3.2108	+0.0071
Muon-NSR ($\gamma = 10$)	3.2000	+0.0178
Muon-NSR ($\gamma = 100$)	3.1984	+0.0194
Muon-NSR ($\gamma = 1000$)	3.1982	+0.0196
Muon-NSR ($\gamma = 10000$)	3.1991	+0.0187

Across both model scales, Muon-NSR consistently outperforms the baselines for a wide range of γ values, confirming the benefit of incorporating variance-adaptive information into the update direction prior to Newton–Schulz orthogonalization. We observe that performance follows a unimodal trajectory with respect to γ : strictly improving as γ increases from small values, reaching an optimum, and then exhibiting mild degradation at excessively large values. Notably, the optimal γ appears to be regime-dependent, peaking at $\gamma = 10$ for GPT-2 and $\gamma = 1000$ for LLaMA-130M. Consequently, we adopt these optimal settings for all subsequent experiments.

Ordering of NSR modulation. A core design principle of Muon-NSR is to apply the variance-adaptive modulation *prior to* the Newton–Schulz orthogonalization. To evaluate the criticality of this ordering, we introduce an ablation variant, **Muon-NSR-Reshuffled**, which reverses the operation sequence and appears to be a more direct analogical extension of (9). Specifically, this variant first computes the standard orthogonalized direction $O_t = \mathbf{NS}_K(\tilde{M}_t)$ and subsequently applies the NSR coordinate-wise rescaling to O_t . The modified update rule is given by:

$$S_t \leftarrow \sqrt{1 + \gamma \frac{\hat{\Gamma}_t}{\tilde{M}_t^{\odot 2} + \varepsilon}}, \quad O_t^{post} = O_t \oslash S_t,$$

where \oslash denotes element-wise division, and O_t^{post} replaces O_t in the parameter update. All other algorithmic components remain identical to Muon-NSR. (See Appendix B for full pseudocode).

The validation trajectories for Llama-130M are compared in Figure 5. Consistent with our main results, **Muon-NSR** (Pre-Ortho) maintains a superior validation loss trajectory over the Muon baseline throughout the entire training process. In contrast, **Muon-NSR-Reshuffled** (Post-Ortho) ex-

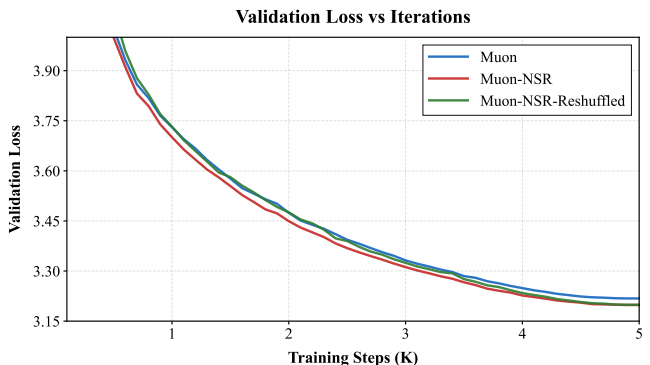


Figure 5: Ablation study on the sequence of NSR modulation for **LLaMA-130M**, comparing **Muon-NSR** (pre-orthogonalization) and **Muon-NSR-Reshuffled** (post-orthogonalization) variants.

hibits distinct phase-dependent behavior: it initially underperforms the Muon baseline, only overtaking it in the mid-to-late training stages. While it eventually converges to a loss value competitive with Muon-NSR, the standard Muon-NSR remains marginally superior at the end of training. These findings suggest that modulating the gradient variance *before* orthogonalization is crucial for consistent optimization gains. Theoretically, applying modulation *after* orthogonalization is suboptimal because it directly perturbs the orthogonality of the Newton–Schulz output (O_t), thereby weakening the spectral constraints that underpin the stability of Muon. Consequently, we adopt the pre-orthogonal modulation design for the proposed algorithm.

5.4 Regime sensitivity and limitations.

We observe that the effectiveness of our variance-adaptive variants depends on large batch sizes to ensure stable gradient statistics. In Suite B, Wen *et al.* [2025] used the same batch size for the LLaMA-130M, 300M, and 520M models. Our methods perform better on LLaMA-130M and 300M models, but worse on LLaMA-520M than the Muon baseline. However, for LLaMA-1.2B, when Wen *et al.* [2025] increased the batch size, our variants outperform the baseline again. Since efficient pretraining typically uses large batches, this sensitivity does not pose a practical limitation [McCandlish *et al.*, 2018; Kaplan *et al.*, 2020].

6 Conclusion

In this work, we introduce **Muon-NSR** and **Muon-VS**, two variance-adaptive extensions of the Muon optimizer. These methods integrate Adam-style variance statistics into the orthogonal update construction while preserving strict spectral control. **Muon-NSR** employs an explicit noise-to-signal (NSR) modulation governed by a tunable sensitivity parameter, whereas **Muon-VS** utilizes a parameter-free variance scaling. Extensive evaluations on GPT-2 and LLaMA pre-training demonstrate that both variants consistently accelerate convergence and achieve lower validation losses compared to robust AdamW and Muon baselines.

References

Jeremy Bernstein, Yu-Xiang Wang, Kamyar Azizzadeh, and Animashree Anandkumar. signsd: Compressed optimisation for non-convex problems. In *International conference on machine learning*, pages 560–569. PMLR, 2018.

Tom Brown, Benjamin Mann, Nick Ryder, Melanie Subbiah, Jared D Kaplan, Prafulla Dhariwal, Arvind Neelakantan, Pranav Shyam, Girish Sastry, Amanda Askell, et al. Language models are few-shot learners. *Advances in neural information processing systems*, 33:1877–1901, 2020.

Xiangning Chen, Chen Liang, Da Huang, Esteban Real, Kaiyuan Wang, Hieu Pham, Xuanyi Dong, Thang Luong, Cho-Jui Hsieh, Yifeng Lu, et al. Symbolic discovery of optimization algorithms. *Advances in neural information processing systems*, 36:49205–49233, 2023.

Lizhang Chen, Jonathan Li, and Qiang Liu. Muon optimizes under spectral norm constraints. *arXiv preprint arXiv:2506.15054*, 2025.

Gheorghe Comanici, Eric Bieber, Mike Schaeckermann, Ice Pasupat, Noveen Sachdeva, Inderjit Dhillon, Marcel Blissein, Ori Ram, Dan Zhang, Evan Rosen, et al. Gemini 2.5: Pushing the frontier with advanced reasoning, multimodality, long context, and next generation agentic capabilities. *arXiv preprint arXiv:2507.06261*, 2025.

John Duchi, Elad Hazan, and Yoram Singer. Adaptive subgradient methods for online learning and stochastic optimization. *Journal of machine learning research*, 12(7), 2011.

Aaron Gokaslan, Vanya Cohen, Ellie Pavlick, and Stefanie Tellex. Openwebtext corpus, 2019.

Daya Guo, Dejian Yang, Haowei Zhang, Junxiao Song, Peiyi Wang, Qihao Zhu, Runxin Xu, Ruoyu Zhang, Shirong Ma, Xiao Bi, et al. Deepseek-r1 incentivizes reasoning in llms through reinforcement learning. *Nature*, 645(8081):633–638, 2025.

Vineet Gupta, Tomer Koren, and Yoram Singer. Shampoo: Preconditioned stochastic tensor optimization. In *International Conference on Machine Learning*, pages 1842–1850. PMLR, 2018.

Jordan Hoffmann, Sebastian Borgeaud, Arthur Mensch, Elena Buchatskaya, Trevor Cai, Eliza Rutherford, Diego de Las Casas, Lisa Anne Hendricks, Johannes Welbl, Aidan Clark, et al. Training compute-optimal large language models. *arXiv preprint arXiv:2203.15556*, 2022.

Keller Jordan, Yuchen Jin, Vlado Boza, Jiacheng You, Franz Cesista, Laker Newhouse, and Jeremy Bernstein. Muon: An optimizer for hidden layers in neural networks, 2024.

Jared Kaplan, Sam McCandlish, Tom Henighan, Tom B Brown, Benjamin Chess, Rewon Child, Scott Gray, Alec Radford, Jeffrey Wu, and Dario Amodei. Scaling laws for neural language models. *arXiv preprint arXiv:2001.08361*, 2020.

Andrej Karpathy. nanopt, 2022. GitHub repository.

Diederik P Kingma. Adam: A method for stochastic optimization. *arXiv preprint arXiv:1412.6980*, 2014.

Frederik Kunstner, Jacques Chen, Jonathan Wilder Lavington, and Mark Schmidt. Noise is not the main factor behind the gap between sgd and adam on transformers, but sign descent might be. *arXiv preprint arXiv:2304.13960*, 2023.

Valentin Leplat, Sergio Mayorga, Roland Hildebrand, and Alexander Gasnikov. Norm-constrained flows and sign-based optimization: Theory and algorithms, 2025.

Zichong Li, Liming Liu, Chen Liang, Weizhu Chen, and Tuo Zhao. Normuon: Making muon more efficient and scalable. *arXiv preprint arXiv:2510.05491*, 2025.

Kaizhao Liang, Lizhang Chen, Bo Liu, and Qiang Liu. Cautious optimizers: Improving training with one line of code. *arXiv preprint arXiv:2411.16085*, 2024.

Jingyuan Liu, Jianlin Su, Xingcheng Yao, Zhejun Jiang, Guokun Lai, Yulun Du, Yidao Qin, Weixin Xu, Enzhe Lu, Junjie Yan, et al. Muon is scalable for llm training. *arXiv preprint arXiv:2502.16982*, 2025.

Ilya Loshchilov and Frank Hutter. Decoupled weight decay regularization. *arXiv preprint arXiv:1711.05101*, 2017.

James Martens and Roger Grosse. Optimizing neural networks with kronecker-factored approximate curvature, 2020.

Sam McCandlish, Jared Kaplan, Dario Amodei, and OpenAI Dota Team. An empirical model of large-batch training, 2018.

Antonio Orvieto and Robert Gower. In search of adam’s secret sauce. *arXiv preprint arXiv:2505.21829*, 2025.

Guilherme Penedo, Hynek Kydlíček, Anton Lozhkov, Margaret Mitchell, Colin A Raffel, Leandro Von Werra, Thomas Wolf, et al. The fineweb datasets: Decanting the web for the finest text data at scale. *Advances in Neural Information Processing Systems*, 37:30811–30849, 2024.

Boris T Polyak. Some methods of speeding up the convergence of iteration methods. *Ussr computational mathematics and mathematical physics*, 4(5):1–17, 1964.

Alec Radford, Jeffrey Wu, Rewon Child, David Luan, Dario Amodei, Ilya Sutskever, et al. Language models are unsupervised multitask learners. *OpenAI blog*, 1(8):9, 2019.

Colin Raffel, Noam Shazeer, Adam Roberts, Katherine Lee, Sharan Narang, Michael Matena, Yanqi Zhou, Wei Li, and Peter J Liu. Exploring the limits of transfer learning with a unified text-to-text transformer. *Journal of machine learning research*, 21(140):1–67, 2020.

Herbert Robbins and Sutton Monro. A stochastic approximation method. *The annals of mathematical statistics*, pages 400–407, 1951.

Frank Schneider, Lukas Balles, and Philipp Hennig. Deepobs: A deep learning optimizer benchmark suite. *arXiv preprint arXiv:1903.05499*, 2019.

Andrei Semenov, Matteo Pagliardini, and Martin Jaggi. Benchmarking optimizers for large language model pre-training. *arXiv preprint arXiv:2509.01440*, 2025.

Chongjie Si, Debing Zhang, and Wei Shen. Adamuon: Adaptive muon optimizer, 2025.

Jianlin Su, Murtadha Ahmed, Yu Lu, Shengfeng Pan, Wen Bo, and Yunfeng Liu. Roformer: Enhanced transformer with rotary position embedding. *Neurocomputing*, 568:127063, 2024.

Tijmen Tieleman and Geoffrey Hinton. Rmsprop: Divide the gradient by a running average of its recent magnitude. coursera: Neural networks for machine learning. *COURSERA Neural Networks Mach. Learn*, 17:6, 2012.

Nikhil Vyas, Depen Morwani, Rosie Zhao, Mujin Kwun, Itai Shapira, David Brandfonbrener, Lucas Janson, and Sham Kakade. Soap: Improving and stabilizing shampoo using adam. *arXiv preprint arXiv:2409.11321*, 2024.

Jinbo Wang, Mingze Wang, Zhanpeng Zhou, Junchi Yan, Lei Wu, et al. The sharpness disparity principle in transformers for accelerating language model pre-training. *arXiv preprint arXiv:2502.19002*, 2025.

Kaiyue Wen, David Hall, Tengyu Ma, and Percy Liang. Fantastic pretraining optimizers and where to find them. *arXiv preprint arXiv:2509.02046*, 2025.

An Yang, Anfeng Li, Baosong Yang, Beichen Zhang, Binyuan Hui, Bo Zheng, Bowen Yu, Chang Gao, Chengan Huang, Chenxu Lv, et al. Qwen3 technical report. *arXiv preprint arXiv:2505.09388*, 2025.

Zhewei Yao, Amir Gholami, Sheng Shen, Mustafa Mustafa, Kurt Keutzer, and Michael W. Mahoney. Adahessian: An adaptive second order optimizer for machine learning, 2021.

Jingzhao Zhang, Sai Praneeth Karimireddy, Andreas Veit, Sungyeon Kim, Sashank Reddi, Sanjiv Kumar, and Suvrit Sra. Why are adaptive methods good for attention models? *Advances in Neural Information Processing Systems*, 33:15383–15393, 2020.

A Additional Experimental Details

Overview and compute environment. This section details the experimental framework for our GPT-2 (nanoGPT) and LLaMA-style (Suite A and Suite B) pretraining benchmarks. We provide comprehensive specifications regarding model architectures, data preprocessing pipelines, training budgets, batching strategies, optimizer hyperparameters, and evaluation metrics. All experiments were conducted on a single node equipped with $8 \times$ NVIDIA RTX 5090 GPUs utilizing Distributed Data Parallel (DDP). To facilitate reproducibility, the complete codebase and configuration files are publicly available at <https://github.com/jingru-lee/Variance-Adaptive-Muon>.

A.1 NanoGPT (GPT-2) Pretraining Setup

Our GPT-2 pretraining experiments utilize the AdaMuon codebase Si *et al.* [2025], which extends the standard nanoGPT Karpathy [2022] implementation of the GPT-2 architecture Radford *et al.* [2019] by incorporating architectural enhancements consistent with Si *et al.* [2025]. These modifications include removing bias terms from linear layers, employing GELU activations, disabling dropout, and replacing learned positional embeddings with Rotary Positional Embeddings (RoPE) Su *et al.* [2024]. We evaluate two model scales, GPT-2 Small and GPT-2 Medium, with detailed configurations provided in Table 3. Adhering to the training protocol described in Si *et al.* [2025], we substitute the standard cosine decay with a warmup-stable schedule comprising a linear warmup phase followed by a constant learning rate.

Data. We train on the OpenWebText corpus Gokaslan *et al.* [2019] using the standard GPT-2 BPE tokenizer. We report language-modeling loss on the held-out validation split.

Training budget and batching. We trained all models on 8 GPUs using Distributed Data Parallel (DDP) for 100,000 optimization steps. By employing gradient accumulation to fix the per-device batch size at 60, we achieved a global batch size of 480 sequences. With a sequence length of 1024, this configuration yields a total training budget of approximately 4.92×10^{10} tokens. Additional hyperparameters include a 2,000-step warmup, bfloat16 mixed precision, and global gradient-norm clipping at 1.0.

Optimizers and hyperparameters. We compare AdamW Loshchilov and Hutter [2017], Muon Jordan *et al.* [2024]; Liu *et al.* [2025], AdaMuon Si *et al.* [2025], with our variants Muon-NSR and Muon-VS. All methods use the same learning rate schedule, with a peak learning rate of 6×10^{-4} and weight decay of 0.1. AdamW uses $(\beta_1, \beta_2) = (0.9, 0.95)$. For Muon-family methods, we consistently apply the standard hybrid parameter partitioning strategy established in prior work Jordan *et al.* [2024]; Si *et al.* [2025] across all experimental setups (NanoGPT, Suite A, and Suite B). Under this scheme, matrix-shaped (2D) parameters within Transformer blocks are optimized using the corresponding Muon-style optimizer, while embedding tables and all vector-shaped (1D) parameters are updated via AdamW. Specific to the GPT-2 experiments, the Muon component utilizes a momentum of 0.95, and the background AdamW optimizer

Table 3: GPT-2 model configurations used in our nanoGPT pre-training experiments.

Model	Layers	Heads	Hidden size	Parameters
GPT-2 Small	12	12	768	124M
GPT-2 Medium	24	16	1024	350M

shares the same learning rate schedule. For the orthogonalized updates, we employ a scaling factor of $s_{\text{scale}} = 0.2\sqrt{\max(m, n)}$, where m and n denote the dimensions of the parameter matrix. For Muon-NSR, we set the NSR sensitivity to $\gamma = 10$ in all nanoGPT experiments.

A.2 Suite A Llama Pretraining Setup

We adhere to the Suite A benchmark framework established by Semenov *et al.* [2025]. All models in this suite employ a decoder-only Llama architecture, incorporating SwiGLU feed-forward blocks, RMSNorm ($\epsilon = 10^{-5}$), and rotary positional embeddings (RoPE). We utilize tied input-output embeddings and exclude both dropout and bias terms from linear layers. Parameters are initialized from a truncated Gaussian distribution ($\sigma = 0.02$). Detailed model specifications and pretraining hyperparameters are summarized in Table 4.

Data and preprocessing. We pretrain on the FineWeb sample-100BT subset Penedo *et al.* [2024]. Following standard benchmarking protocols, the corpus is tokenized and partitioned into training and validation sets. For tokenization, we employ the GPT-2 tokenizer (vocabulary size 50,304) with a fixed context length of 512 tokens for both training and evaluation.

Optimization and learning-rate schedule. We utilize AdamW-style decoupled weight decay with a coefficient $\lambda = 0.1$ and apply global gradient-norm clipping. We employ a linear warmup of 2,000 steps to the peak learning rate, followed by a cosine decay schedule, decaying to a minimum of $0.01 \times$ peak learning rate.

Optimizers compared. We benchmark our proposed algorithms, **Muon-NSR** and **Muon-VS**, against the established AdamW and standard Muon baselines under identical model, data, and schedule settings. AdamW uses $(\beta_1, \beta_2) = (0.9, 0.999)$ for *Llama-210M* and $(0.9, 0.99)$ for *Llama-720M*, with $\epsilon_{\text{adam}} = 10^{-8}$. For Muon-family methods, we follow the benchmark’s distributed implementation with momentum $\beta_{\text{muon}} = 0.95$ and Nesterov acceleration. We approximate the polar factor using Newton–Schulz iterations ($T_{\text{NS}} = 5$). Consistent with the standard Muon formulation, we apply an update scaling factor defined by $s_{\text{scale}} = 0.2\sqrt{\max(m, n)}$. For Muon-NSR, we use the default variance-sensitivity coefficient $\gamma = 1000$.

Evaluation protocol. We evaluate all pretrained models on a fixed subset of the validation split to ensure consistency across experimental runs. We report *validation loss*, defined as the mean token-level cross-entropy. Additionally, for Suite A, we report *next-token top-1 accuracy*, which measures the fraction of token positions where the model’s most probable prediction matches the ground truth.

Table 4: **Suite A Llama-style pretraining configuration.** Abbreviations: **Hid**: Hidden size; **L**: Layers; **H**: Attention heads; **Sch**: Schedule; **WU**: Warmup steps; **Tok**: Total training tokens; **WD**: Weight decay; **Clip**: Gradient norm clip; **Peak**: Peak learning rate.

Model	Hid	L	H	Batch	Steps	Tok	Sch	WU	Peak	WD	Clip
Llama-210M	768	24	12	256	128k	16.8B	cos	2k	10^{-3}	0.1	0.5
Llama-720M	2048	12	16	1984	48k	48.0B	cos	2k	10^{-3}	0.1	0.1

Table 5: **Suite B pretraining specifications and optimizer hyperparameters.** All models employ 32 Transformer layers with a context length of 4096. **BSZ** denotes the global batch size; **Clip** refers to the global gradient-norm clipping threshold; and **WSD** indicates the decay-stage length within the warmup–stable–decay schedule Wen *et al.* [2025].

Model	Hid	FFN	Heads	BSZ	η_{adam}	$\eta_{\mu\text{on}}$	$\beta_{\mu\text{on}}$	Clip	(β_1, β_2)	ϵ_{adam}	WSD	Sch	WU	η_{\min}
Llama-130M	512	2048	8	128	0.0032	0.016	0.95	1.0	(0.8, 0.98)	10^{-15}	0.8	linear	0	0
Llama-300M	768	3072	12	128	0.0024	0.008	0.98	1.0	(0.8, 0.98)	10^{-15}	0.8	linear	0	0
Llama-1.2B	1536	6144	24	256	0.0012	0.008	0.98	2.0	(0.8, 0.98)	10^{-25}	1	linear	0	0

A.3 Suite B LLaMA Pretraining Setup

We conduct our *Suite B* experiments using the LLaMA architecture. To ensure fair benchmarking, we adopt the pretraining protocol of Wen *et al.* [2025], which prioritizes regime-specific hyperparameter optimization. Our implementation utilizes the codebase from Liang *et al.* [2024], reproducing the training recipes and learning rate schedules of Wen *et al.* [2025] under $1\times$ Chinchilla token budget. Table 5 summarizes the training budget and optimizer hyperparameters.

Model Architecture. We pretrain three decoder-only models based on the LLaMA architecture: LLaMA-130M, LLaMA-300M, and LLaMA-1.2B. To isolate the impact of width, we maintain a *fixed depth* of 32 layers and a sequence length of 4,096 tokens across all model scales. Table 5 provides the detailed architectural specifications.

Data and Preprocessing. Distinct from the multi-source data mixture employed in Wen *et al.* [2025], we pretrain exclusively on the DCLM dataset. This decision is justified by the fact that DCLM constitutes the vast majority ($> 90\%$) of the reference corpus, effectively allowing us to reproduce the primary findings with reduced complexity. We utilize the LLaMA-2 tokenizer for corpus processing and adopt the sequence packing and token-stream preprocessing protocols of the reference implementation. All downstream evaluations are performed on the C4-en validation split.

Optimizers and Hyperparameters. We benchmark Muon against our proposed variants, Muon-NSR and Muon-VS. To strictly isolate the efficacy of our algorithmic modifications, the variants *retain* the base Muon hyperparameters without undergoing separate tuning. Specifically for Muon-NSR, we introduce a sensitivity coefficient of $\gamma = 1000$. For the update magnitude, we adopt the scaling rule $s_{\text{scale}} = \sqrt{\max(1, m/n)}$ in accordance with Wen *et al.* [2025], ensuring alignment with their established tuning protocol.

B Additional Algorithms

Muon-NSR-Reshuffled. To assess whether NSR modulation should be *before* or *after* Newton–Schulz (NS)

Algorithm 2 Muon-NSR-Reshuffled

Require: Parameters $W_0 \in \mathbf{R}^{m \times n}$; learning rate η ; weight decay λ ; EMA rate β (shared for first and second moments, i.e., $\beta_1 = \beta_2 = \beta$); variance-sensitivity γ ; stabilizer ε ; Newton–Schulz iterations K .

- 1: $M_0 \leftarrow 0$, $\Gamma_0 \leftarrow 0$
- 2: **for** $t = 1, 2, \dots$ **do**
- 3: $G_t = \text{Stochastic Gradient Oracle}(W_{t-1})$
- 4: $\Gamma_t \leftarrow \beta\Gamma_{t-1} + \beta(1 - \beta)(M_{t-1} - G_t)^{\odot 2}$
- 5: $M_t \leftarrow \beta M_{t-1} + (1 - \beta)G_t$
- 6: $\widehat{M}_t \leftarrow \frac{M_t}{1 - \beta^t}$, $\widehat{\Gamma}_t \leftarrow \frac{\Gamma_t}{1 - \beta^t}$
- 7: $\tilde{M}_t \leftarrow G_t + \frac{\beta}{1 - \beta} \widehat{M}_t$
- 8: $O_t \leftarrow \text{NS}_K(\tilde{M}_t)$
- 9: $S_t \leftarrow \sqrt{1 + \gamma \frac{\widehat{\Gamma}_t}{\tilde{M}_t^{\odot 2} + \varepsilon}}$ {elementwise}
- 10: $O_t^{\text{post}} \leftarrow O_t \oslash S_t$ {elementwise}
- 11: $W_t \leftarrow W_{t-1}(1 - \eta\lambda) - \eta s_{\text{scale}} O_t$
- 12: **end for**

orthogonalization, we introduce a reshuffled ablation, *Muon-NSR-Reshuffled* (detailed in Algorithm 2). Unlike the original Muon-NSR pipeline that applies noise-to-signal ratio (NSR) modulation to the update proxy prior to orthogonalization, this variant first orthogonalizes the extrapolated first-moment proxy \tilde{M}_t to obtain a semi-orthogonal direction $O_t = \text{NS}_K(\tilde{M}_t)$ and subsequently applies NSR attenuation via coordinate-wise scaling. Concretely, we define the elementwise scaling factor

$$S_t \leftarrow \sqrt{1 + \gamma \frac{\widehat{\Gamma}_t}{\tilde{M}_t^{\odot 2} + \varepsilon}}$$

and compute the modulated direction via elementwise division, $O_t^{\text{post}} = O_t \oslash S_t$. Because post-orthogonalization coordinate-wise scaling, in general, is not orthogonality-preserving, this step can violate the orthogonality of O_t and thus relax the spectral constraint enforced by Muon. Consequently, we employ Muon-NSR-Reshuffled strictly as an

Table 6: Hyperparameter sweep over the NSR variance-sensitivity coefficient γ for **Muon-NSR-Reshuffled** on Suite B **LLaMA-130M**. We report the final validation loss at the end of training. Selected results are highlighted in **bold**.

Optimizer	Final Val Loss
Muon (Baseline)	3.2179
Muon-NSR ($\gamma = 1000$)	3.1982
Muon-NSR-Reshuffled ($\gamma = 0.1$)	3.2149
Muon-NSR-Reshuffled ($\gamma = 1$)	3.2068
Muon-NSR-Reshuffled ($\gamma = 10$)	3.1989
Muon-NSR-Reshuffled ($\gamma = 100$)	3.2057

ablation baseline to empirically validate the ordering of NSR modulation relative to NS orthogonalization, rather than as a proposed standalone optimizer.

Experimental setup for the ablation. We conduct ablation studies using the LLaMA-130M configuration following the Suite B pretraining protocol (Section A.3). Specifically, we perform a grid search over the NSR variance-sensitivity coefficient, $\gamma \in \{0.1, 1, 10, 100\}$, while keeping all other hyperparameters fixed. As reported in Table 6, the reshuffled variant achieves optimal performance at $\gamma = 10$, yielding a final validation loss of 3.1989. This result is comparable to the standard Muon-NSR configuration (3.1982) and significantly outperforms the unmodulated Muon baseline (3.2179). However, the training dynamics of Muon-NSR-Reshuffled are analyzed in detail in Section 5.3 of the main text, which discusses the characteristic behavior of delayed early convergence followed by mid-to-late stage acceleration.